Development of a Scaled Conjugate Gradient Algorithm for Significant RF Neural Signal Processing

Muhammad Farid Akmal Mohd Norden, Roshakimah Mohd Isa*, Mohd Roshalizi Mohd Isa, Ros Shilawani S. Abdul Kadir, Muhammad Hariz Md Azli and Amir Syarif Muhammad Akram

Abstract—Artificial Neural Networks (ANN) are computational models inspired by the human brain, capable of recognizing patterns and making predictions. Scale Conjugate Gradient (SCG) algorithm is an efficient training method for ANN that accelerates the learning process and improves output accuracy. However, conventional ANN training methods often struggle with slow convergence and can be less accurate when analyzing complex, high-dimensional data such as Electroencephalogram (EEG) signals. Furthermore, the precise classification of subtle neural pattern changes induced by Radiofrequency (RF) exposure remains a significant challenge. SCG improves the learning process of ANNs by speeding up the adjustment of their internal weights, helping the network learn faster and more accurately from large data sets. This study aims to improve the classification of RF neural data patterns using SCG. EEG neural data was captured in sessions before, during and after RF exposure. Power Asymmetry Ratio (PAR) was used for feature extraction. The data involved 96 subjects, were split into 70:30 ratio for training and testing in ANN modelling. The SCG algorithm was integrated, initialized with one hidden layer of 10 neurons. Parameter adjustments were made to optimize convergence, potentially involving multiple layers for model refinement. The results show that RF exposure in During session produces significantly distinct neural patterns, enabling the highest ANN classification accuracy.

Index Terms—Brainwave, classification, feature extraction, neural signal, Scale Conjugate Gradient (SCG)

I. INTRODUCTION

Artificial Neural Networks (ANN) process information in a manner analogous to the human brain. They consist of layers of interconnected neurons, each of which receives inputs and produces outputs [1]. ANNs are non-linear mapping systems

This manuscript is submitted on 18^{th} August 2025, revised on 12^{th} September 2025, accepted on 22^{nd} September 2025 and published on 31^{st} October 2025.

Muhammad Farid Akmal Mohd Norden completed his degree at Universiti Teknologi MARA. His project was supervised by Dr. Roshakimah Mohd Isa, who is currently with the Faculty of Mechanical Engineering, Universiti Teknologi MARA. Mohd Roshalizi Mohd Isa is now affiliated with Kuantan Community College, Malaysia. Ros Shilawani S. Abdul Kadir is currently with the Faculty of Electrical Engineering, Universiti Teknologi MARA. Muhammad Hariz Md Azli and Amir Syarif Muhammad Akram have completed their degree at Universiti Teknologi MARA

*Corresponding author Email address: roshakimah@uitm.edu.my

1985-5389/© 2023 The Authors. Published by UiTM Press. This is an open access article under the CC BY-NC-ND license (http://creativecommons.org/licenses/by-nc-nd/4.0/).

structured similarly to human neural networks [2]. An artificial neuron is the fundamental building component of any ANN, using basic mathematical model comprising multiplication, summation, and activation [3]. The connection strength from an input to a neuron is noted by the value of the weight [2]. The connections between neurons vary in strength, either exciting or inhibiting, and this strength difference affects information flow [1]. Negative weight values reflect inhibitory connections, while positive values designate excitatory connections [2]. Neurons can be grouped into layers: input, hidden, and output layers. The connections and the way these layers interact play a crucial role in solving specific problems [1].

II. LITERATURE REVIEW

Electroencephalogram (EEG) is an instrument used to record brain electrical activity as an analogue signal. There are three techniques used to record the brain signal: invasive, partially invasive, and non-invasive, which is EEG [4]. It has a wide range of applications, from clinical diagnostics to brain-triggered neurorehabilitation treatments [5]. The technique records the net difference in voltage activity between ionic current flows in the brain, which is controlled by NMDA glutamate receptors [6]. EEG can be measured by placing the electrodes directly on the cortex or on the scalp. EEG rhythm data is classified into five different frequencies which are delta (0.5–4 Hz), theta (4–8 Hz), alpha (8–13 Hz), beta (13–30 Hz), and gamma (above 30 Hz) [7].

After extracting raw data of brain activity through EEG, the data will undergo artifact and noise removal as EEG preprocessing before applying Fast-Fourier Transform (FFT). FFT as an advanced digital signal processing technique is used to help with the classification of brainwave and feature extraction of EEG signal [8]. According to [9], FFT is suitable for a narrowband signal such as sine wave. It is a good tool for stationary signal processing and in real-time applications, FFT has a better speed compared to all other available methods virtually. Noise is neurological activities that are not relevant in examining the behavioral task, and artifact is an external activity that is not related to neurological activities such as electrical interference, eye movement, or respiration [10]. The artifacts may come from measurement instruments such as faulty electrodes, line noise, and high electrode impedance, which can be reduced or avoided by using a high-node precision equipment and standardized procedure of recording, while physiological artifacts which come from human subjects are

harder and more complicated to remove [11].

For characterizing EEG data, there are two common approaches performed on functional correlation (FC) patterns which is Power Spectral Density (PSD) and network analysis [12]. PSD is usually computed using a parametric autoregressive (AR) model where it provides signal power information at relatively narrow frequency sub-bands [13]. SCG algorithm has been shown to be a highly effective method for training artificial neural networks. SCG is particularly suitable for applications such as the classification of electromyographic data [14], automated seizure detection using EEG data [15], and the classification of depressive and normal states in EEG data [16] as it offers fast and more stable convergence. It is faster to converge due to its effectiveness in training deep neural networks [17]. SCG outperforms other gradient-based optimization methods in speed and accuracy in a comparative study [18]. It offers significant performance benefits in neural network training despite the challenges in implementing SCG, such as precise parameter tuning [19]. A confusion matrix is an essential tool for summarizing prediction results in a structured format for evaluating the performance of classification models [20]. Confusion matrix provides insight into the model's accuracy and comprises four components: true positives, true negatives, false positives, and false negatives [21].

III. METHODOLOGY

Fig. 1 presents the flowchart for project methodology. In the comprehensive process of signal processing for the development of the SCG algorithm in RF neural signal processing, data acquisition initiates with the collection of EEG data capturing brain activity in before, during and after the RF exposure session. The EEG neural signals were recorded in time domain, encompassing 5 minutes period of each session for Left Exposure (LE), Right Exposure (RE), and Sham Exposure (SE) across 96 EEG data of subjects per frequency band. Then EEG recording involved two electrodes placed at the forehead to record the frontal hemisphere brainwave signals.

The RF exposure source ranging from 900 MHz to 2.2 GHz with 0.69 W/Kg Specific Absorption Rate (SAR). After data collection, a meticulous filtering stage eliminates artifacts and noise using bandpass and notch filters, employing techniques such as filtering and artifact rejection. Moving to the signal preprocessing phase, a series of steps is undertaken to prepare the data for analysis. The FFT converted the time-domain signal into a frequency-domain signal, providing PSD at different frequency bands, namely alpha, beta, theta, and delta.

The squared magnitude of FFT is then calculated to obtain PSD. Normalization was conducted for the PSD data, focusing on relative power changes within specific frequency bands.

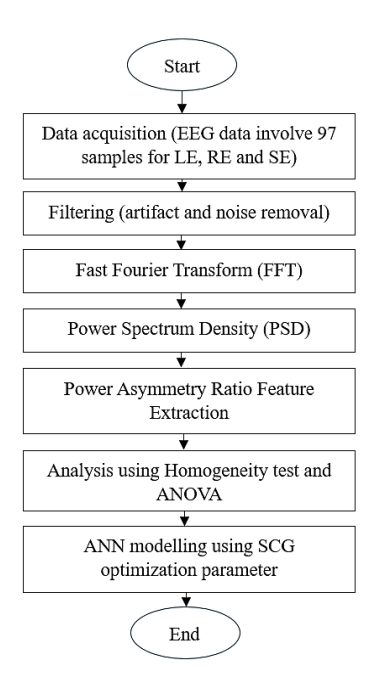


Fig. 1. Methodology flowchart.

This step is crucial in EEG analysis, emphasizing the importance of understanding the relative distribution of power across delta, theta, alpha and beta frequency ranges. The normalization formula given in (1), is applied to scale the PSD values from 0 to 1.

$$X_{normalize} = \frac{X}{Xmax} \tag{1}$$

Feature extraction is conducted using the PAR formula as in (2), capturing both positive and negative values to extract significant behavioral patterns within each frequency band. P_L indicates PSD value for left hemisphere and P_R indicates PSD value for right hemisphere.

$$PAR = \frac{P_L - P_R}{P_L + P_R} \tag{2}$$

Subsequently, pattern recognition is achieved through data visualization by plotting graphs, including box plots and scatter graphs. The signal undergoes the feature extraction and analysis using Analysis of Variance (ANOVA) and Homogeneity Test. Finally, ANN modeling is executed with 70:30 ratio dataset split for training and testing. The SCG algorithm is applied, integrated into the input, hidden layer, and expected output of the neural network. The initial networks configuration involves a single hidden layer with 10 neurons and an input layer with 2 nodes. To optimize convergence, adjustments were made, potentially incorporating multiple hidden layers with varying neuron configurations until convergence is achieved and the model is refined.

IV. RESULTS AND DISCUSSION

A. PAR Analysis for Beta and Alpha

For Beta LE, there is a slight decrease from the Before session to the During session, followed by a slight increase in the After session as shown in Fig. 2. For Beta RE, the mean value slightly increases from the Before session to the During session and decreases in the After session. For Beta SE, the mean value slightly increases from the Before session to the During session, then remains stagnant in the After session. The overall beta mean value shows no significant difference across all sessions for all exposures.

For Alpha LE, there is an increment from the Before session to the During session, followed by a slight decrease in the After session, as illustrated in Fig. 3. For Alpha RE, the mean value remains stagnant throughout all sessions. For Alpha SE, the mean value slightly decreases from the Before session to the During session, then increases in the After session. Alpha LE shows a significant increase compared to other exposures. The mean value for both Alpha and Beta in LE is the highest, indicating for highly left hemisphere dominance.



Fig. 2. PAR Beta between exposure and session.

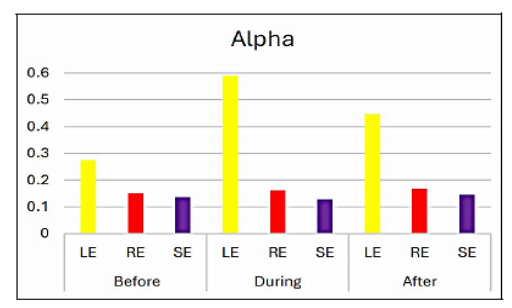


Fig. 3. PAR Alpha between exposure and session.

B. ANOVA Analysis

Significant differences (p < 0.05) were observed in the Before Beta, Before Alpha, During Alpha, After Beta, and After Alpha conditions, suggesting that the experimental stimulus had a statistically significant impact on the subject. From Table 1, the "During Beta" condition did not show significant differences (p = 0.092), indicating that the exposure did not significantly affect the subject during the exposure period. However, further analysis was conducted with ANN to classify the brainwave signals.

TABLE I. ANOVA ANALYSIS OF SIGNIFICANT DIFFERENCE BETWEEN EXPOSURE

Session	Brainwave	Significant, p Value	Remarks
Before	Beta	0.0014	Significant
	Alpha	0.0310	Significant
During	Beta	0.0920	Not Significant
	Alpha	0.0000	Significant
After	Beta	0.0310	Significant
	Alpha	0.0000	Significant

C. MSE vs Hyperparameter

Mean Square Error (MSE) is used to determine the optimal hyperparameters of the ANN Modelling using SCG. The hyperparameters are learning rate and hidden layer size. The hyperparameters were chosen by finding the lowest MSE value across a range of value sets as shown in Fig. 4, 5 and 6.

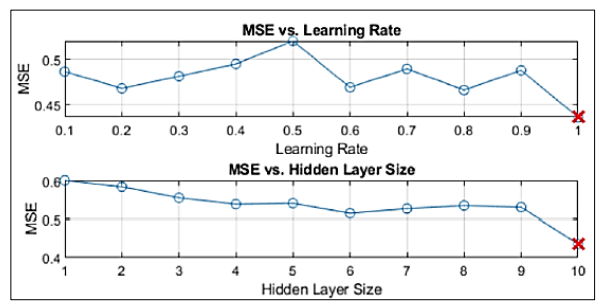


Fig. 4. MSE vs Hyperparameter for Before Session.

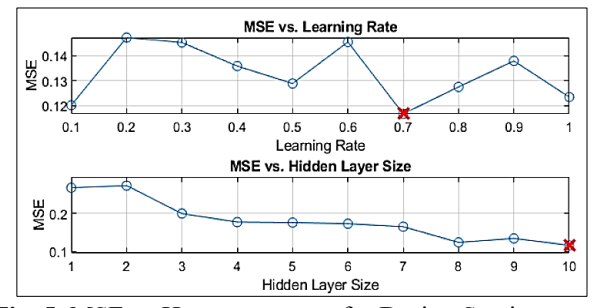


Fig. 5. MSE vs Hyperparameter for During Session.

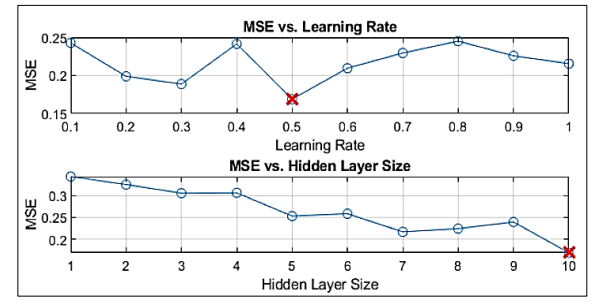


Fig. 6. MSE vs Hyperparameter for After Session.

The analysis of the learning rate throughout different sessions (Before, During, and After) reveals a dynamic and adaptive approach required for optimal neural network training as illustrated in Table 2. Before the exposure, a high learning rate (1.0) enabled significant weight adjustments and balanced exploration in the early training phase. During the session, due

to increased complexity from the RF stimulus, the learning rate was reduced to 0.7, facilitating finer adjustments and leveraging past gradient directions to navigate the more complex error landscape. In the after session, the learning rate further reduced to 0.5, supporting precise weight updates and smooth convergence towards the optimal solution.

TABLE II. LOWEST MSE FOR HYPERPARAMETERS IN EACH SESSION

Parameters	Session: Before	During	After
Learning rate	1.0	0.7	0.5
Hidden Layer	10.0	10.0	10.0

D.PAR ANN Modeling Using SCG

The confusion matrices for Before session as in Fig. 7, show model performance before the exposure to radiofrequency stimulation. Both matrices highlight significant misclassifications among the classes. This indicates the model has difficulty distinguishing between left exposure, right exposure, and sham exposure when the brain has not been influenced by the stimulus. Such results are expected because the data, recorded before exposure, lack distinctive patterns.



Fig. 7. Training and Testing confusion matrix for Before session.

The linear regression line for Before session in Fig. 8 shows that the regression fit (blue line) diverges from the ideal fit (dotted line) for both training and testing data. Such divergence is to be expected as the subject is yet to be exposed to the stimulus. The regression equation on training data indicates that the predicted output increases by 0.33 units for each unit increase in the target, starting from an intercept of 1.3 when the target is zero. For the testing data, the equation indicates that the predicted output increases by 0.017 units for each unit increase in the target.

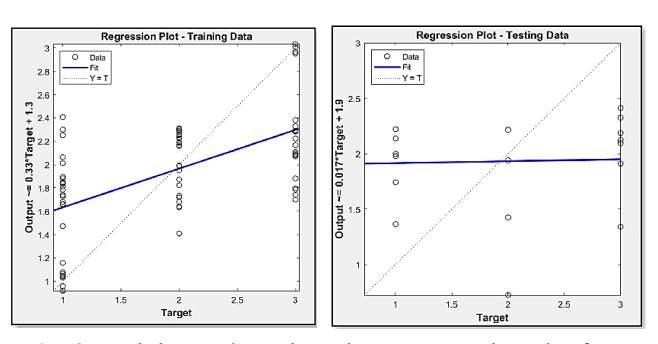


Fig. 8. Training and Testing Linear Regression plot for Before session.

The prediction of training for Before session in Fig. 9 shows the data before undergoing ANN modelling of SCG algorithm and the classification of training shows the data after putting through the ANN modelling where the data aligned to the measured target according to the prediction of the SCG algorithm.

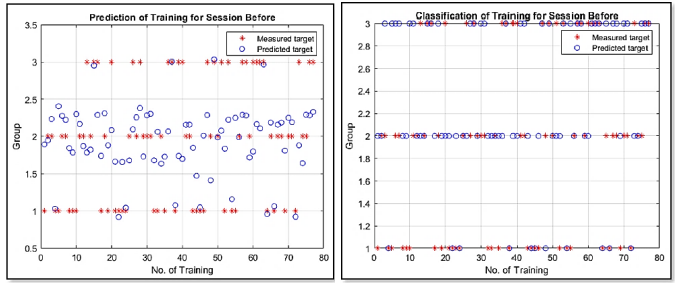


Fig. 9. Prediction and classification of Training for Before session.

The prediction of testing for Before session in Fig. 10 shows the data before undergoing ANN modelling of SCG algorithm and the classification of training shows the data after putting through the ANN modelling where the data aligned to the measured target according to the prediction of the SCG algorithm.

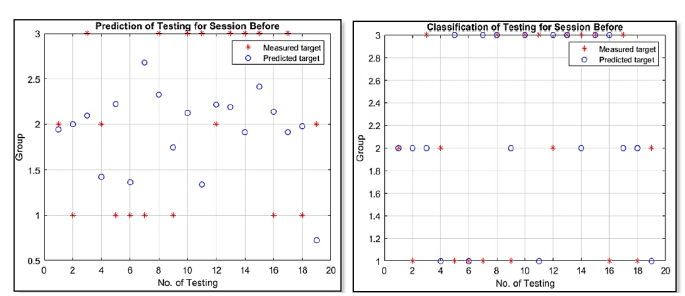


Fig. 10. Prediction and classification of Testing for Before session.

Fig. 11 shows the feature overlap visualisation between groups for Before session of the RF exposure. As observed, the exposures are overlapping each other. This feature overlap is the reason the ANN model had difficulty accurately classifying the data, leading to lower classification accuracy in Before session. As the mobile phone RF has yet to be exposed to the subject, there is no distinct pattern between exposure groups.

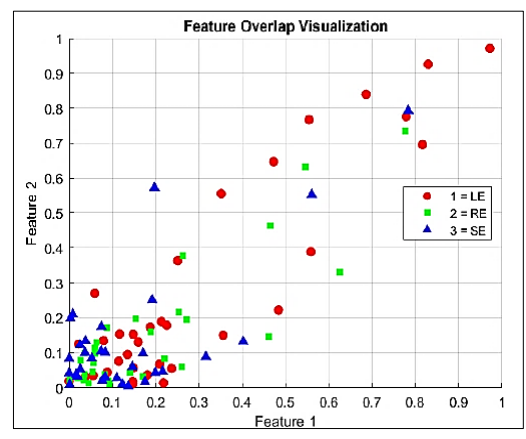


Fig. 11. Data overlap visualisation for Before session.

The confusion matrices for the During session as in Fig. 12 show a significant improvement compared to the Before session. In the During training matrix, it exhibits high accuracy for LE and substantial improvement in correctly identifying the subjects in RE and SE classes. In the During testing matrix, it shows better performance with more accurate classifications across all classes for training and testing accuracy.

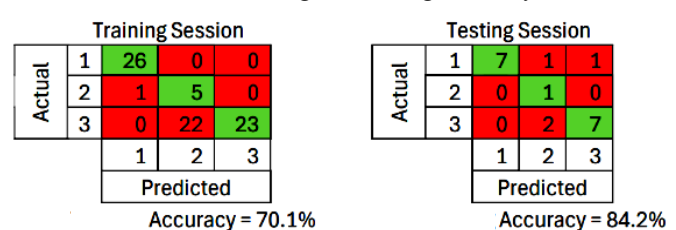


Fig. 12. Training and Testing confusion matrix for During session.

The During session plot in Fig. 13 shows a stronger relationship between the target and output compared to the Before session plot. The slope is significantly higher, and the intercept is lower, suggesting that the model fits the data more closely during the session than before. This indicates an improvement in the regression model's performance during the session.

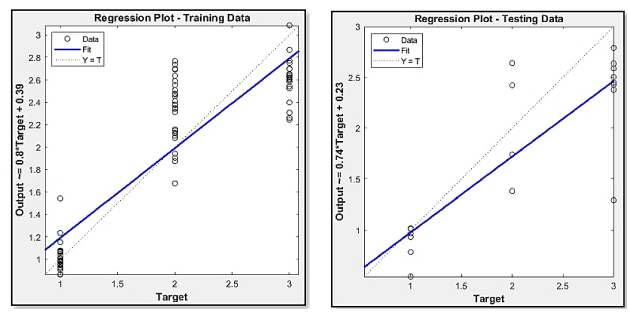


Fig. 13. Training and Testing Linear Regression plot for During session.

The prediction of training for During session as in Fig. 14 shows the data before and the classification of training shows the data after putting through the ANN modelling where the data goes to the measured target according to the prediction of

the SCG algorithm. It shows better prediction in classification of training for During session with more predicted target aligned to the measured target suggesting more accurate prediction. The same applies to testing data as depicted in Fig. 15, where more predicted target accurately classified at the measured target with higher percentage of accuracy after undergoing the SCG algorithm.

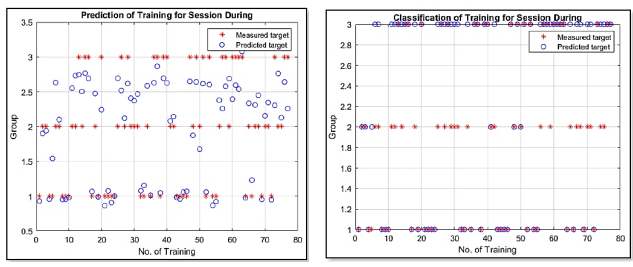


Fig. 14. Prediction and classification of Training for During session.

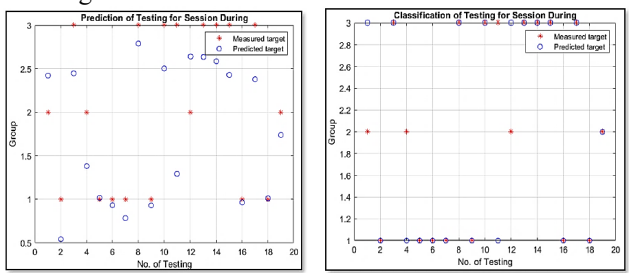


Fig. 15. Prediction and classification of Testing for During session.

Fig.16 shows the feature overlap visualisation. The LE data are well separated while RE and SE value overlap and closely positioned around each other causing more harder for SCG algorithm to classify accurately. Thus, resulted the RE data to be misclassified to SE group. Circles represent LE, rectangles represent RE while triangles represent SE.

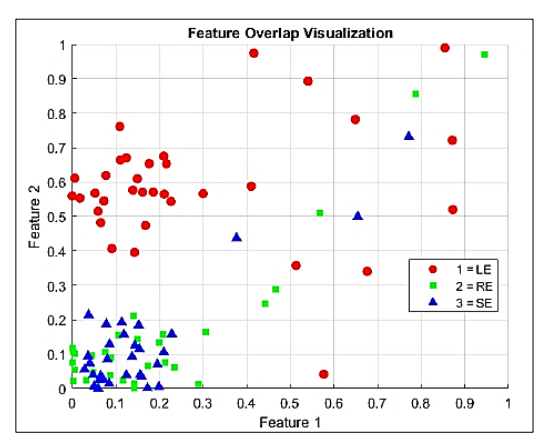


Fig. 16. Data overlap visualisation for During session.

The confusion matrices for the After session as in Fig. 17 show a significant decrease as compared to the During session. This is due to the removal of RF stimulus, therefore resulted the brainwave response decreased.

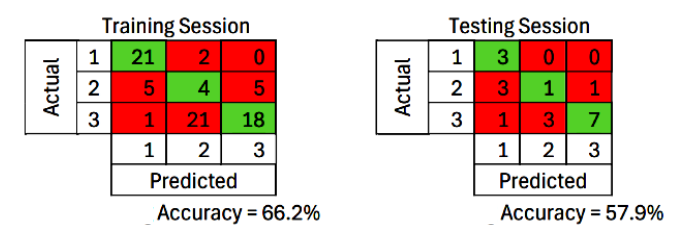
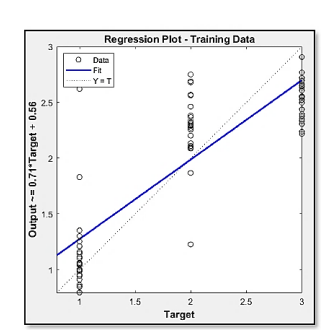


Fig. 17. Training and Testing confusion matrix for After session.

Regression in After session as in Fig. 18 shows a slight decrease in the strength of the relationship between the target and output. The "During Session" plot demonstrates a steeper slope and a lower intercept, indicating a stronger correlation and a lower baseline output. Conversely, the "After Session" plot shows a marginally less steep slope and a higher intercept, suggesting a minor reduction in model performance but still maintaining a relatively strong fit. This indicates that while the predictive power was strongest in During session, it slightly declined afterward, though not significantly enough to undermine its overall effectiveness.



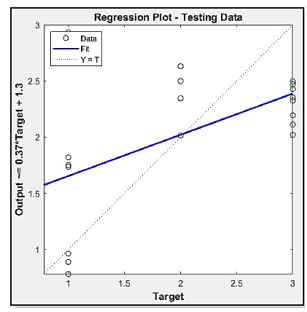
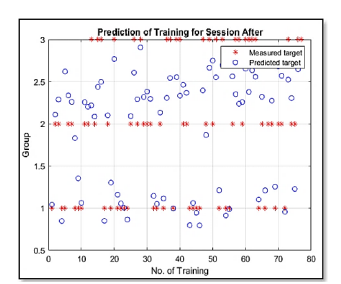


Fig. 18. Training and Testing Linear Regression plot for After session.

The prediction of training for After session as in Fig. 19 shows the data before and the classification of training shows the data after putting through the ANN modelling where the predicted data closely matches the actual measured target as classified by the SCG algorithm. It shows better prediction in classification of training for During session with more predicted target goes to the measured target suggesting more accurate prediction. The same applies to the testing data as in Fig. 20 where predicted target classified with lower accuracy compared to the During session due to the absence of the RF stimulus. This is expected as there were no exposure having by the subjects during the session.

Fig. 21 shows feature overlap visualisation for all exposure groups in After session. It shows how all exposure begins to overlap and closing to each other. This is because the mobile phone RF is removed from the subjects in the After session. As the data overlapped increased, the harder the modelling to accurately classified the data according to their respective classes of exposure.



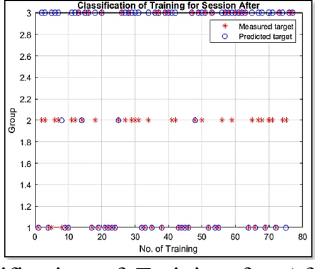
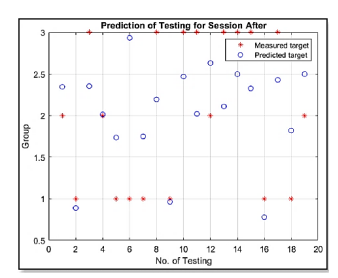


Fig. 19. Prediction and classification of Training for After session.



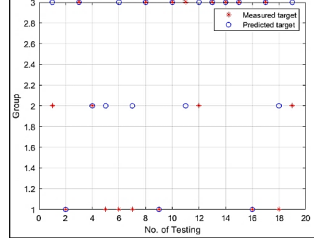


Fig. 20. Prediction and classification of Testing for After session.

Fig. 21 shows feature overlap visualisation for all exposure groups in After session. It shows how all exposure begins to overlap and closing to each other. This is because the mobile phone RF is removed from the subjects in the After session. As the data overlapped increased, the harder the modelling to accurately classified the data according to their respective classes of exposure.

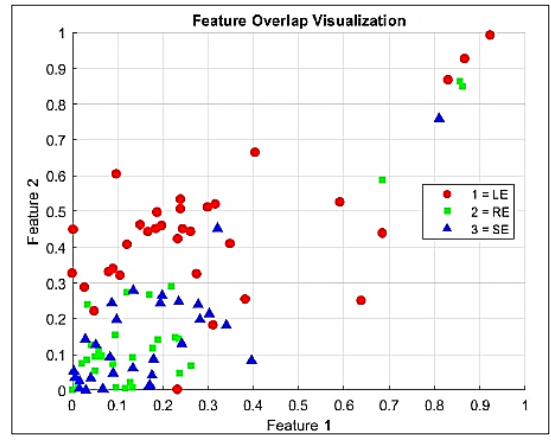


Fig. 21. Data overlap visualization for After session.

The confusion matrices for the Before session demonstrate significant misclassifications, indicating difficulty in distinguishing between different exposure types when the brain is not influenced by the RF stimulus. This lack of stimulus means the brainwave patterns do not have distinct features, leading to lower prediction accuracy. The regression analysis also reflects this with a notable divergence from the ideal fit, expected due to the absence of distinguishable patterns in the data during this session.

During the RF exposure session, there is a notable improvement in classification accuracy as illustrated in Table

4. The confusion matrices indicate significant enhancements, particularly in identifying LE brainwaves. The regression analysis shows a stronger correlation between the predicted outputs and the actual targets, indicating enhanced model performance during RF exposure. The percentage of correct predictions is higher in the During session compared to the Before session, suggesting that the RF stimulus induces distinguishable brainwave patterns. This improvement is evident despite some misclassifications, such as 22 subjects from the RE class being misclassified as SE, likely due to high feature overlap between RE and SE classes. The fit line from the regression analysis converges towards the target during RF exposure, reflecting increased accuracy for both training and testing.

In the After session, there is a slight decrease in accuracy compared to the During session as the RF stimulus is removed. Without the stimulus, the distinct brainwave patterns begin to dissipate, leading to a reduction in classification performance. The regression analysis in the After session shows a minor reduction in model performance but still maintains a relatively strong fit. This suggests that brain activity gradually returns to its baseline state post exposure, resulting in decreased accuracy. Overall, the RF stimulus significantly influences brainwave patterns, enhancing the model's classification performance during exposure, while the after-exposure phase highlights the temporary nature of these induced patterns.

TABLE VI. TRAINING AND TESTING ACCURACY FOR EACH SESSION

Accuracy (%)	Session: Before	During	After
Training	49.4	70.1	66.2
Testing	47.4	84.2	57.9

V. CONCLUSION AND RECOMMENDATION

This research demonstrates the effective application of SCG algorithm for training ANNs in the context of RF neural signal processing. Through comprehensive EEG data acquisition and meticulous preprocessing, the study successfully extracted and analysed neural patterns across various exposure scenarios. The findings reveal that RF exposure impacts brainwave activity, with significant differences observed in the beta and alpha PAR in during and after exposure sessions.

The optimized hyperparameters, identified through MSE analysis, highlight the dynamic adjustment needed in parameters tuning to achieve precise neural network training. The SCG-based ANN models showed varying degrees of accuracy in predicting and classifying brainwave patterns before, during, and after RF exposure, underscoring the complex nature of neural responses to RF stimuli. This research not only advances the understanding of RF neural interactions but also contributes to the development of efficient neural network training methodologies for accurate classification and pattern recognition in biomedical applications. As an enhancement in future work, analysis can be carried out using low-frequency neural signals within the 0-8 Hz range.

VI. ACKNOWLEDGMENT

The authors would like to express their sincere gratitude to the staff and students of Universiti Teknologi MARA, Malaysia, for their valuable contributions and active participation in this research. Their support and involvement were instrumental in ensuring the success of this study.

REFERENCES

- [1] O. Isaac Abiodun, A. Jantan, A. Esther Omolara, K. Victoria Dada, N. AbdElatif Mohamed, and H. Arshad, "State-of-the-art in artificial neural network applications: A survey," Heliyon, vol. 4(11), 2018. doi: 10.1016/j.heliyon.2018.
- [2] A. D. Dongare, R. R. Kharde, and A. D. Kachare, "Introduction to Artificial Neural Network," *International Journal of Engineering and Innovative Technology (IJEIT)*, vol. 2(1), pp 189-194, 2012.
- [3] K. Suzuki, "Artificial neural networks: methodological advances and biomedical applications," *BoD–Books on Demand*, 2011.
- [4] R. Martinek, M. Ladrova, M. Sidikova, R. Jaros, K. Behbehani, R. Kahankova, and A. Kawala-Sterniuk., 2021. "Advanced bioelectrical signal processing methods: Past, present and future approach—Part II: Brain signals," *Sensors*, vo. 21, no. 19, 2021.
- [5] A. Biasiucci, B. Franceschiello, and M. M. Murray, "Electroencephalography," *Current Biology*, vol. 29, no. 3. Cell Press, pp. 80–85, 2019. doi: 10.1016/j.cub.2018.11.052.
- [6] A. Q. Rana, A. T. Ghouse, and R. Govindarajan, "Basics of Electroencephalography (EEG)," *Neurophysiology in Clinical Practice*, pp. 3–9. 2017. doi: 10.1007/978-3-319-39342-1_1.
- [7] K. Blinowska and P. Durka, "ELECTROENCEPHALOGRAPHY (EEG)," Wiley encyclopedia of biomedical engineering, vol. 10, pp. 1-15, 2006.
- [8] R. Jaswal, "Brain Wave Classification and Feature Extraction of EEG Signal by Using FFT on Lab View," International Research Journal of Engineering and Technology, 2016.
- [9] A. S. Al-Fahoum and A. A. Al-Fraihat, "Methods of EEG Signal Features Extraction Using Linear Analysis in Frequency and Time-Frequency Domains," *ISRN Neurosci*, vol. 2014, pp. 1–7, 2014, doi: 10.1155/2014/730218.
- [10] S.-P. Kim, "Preprocessing of EEG," Computational EEG Analysis: Methods and Applications, pp. 15–33, 2018. doi: 10.1007/978-981-13-0908-3 2.
- [11] X. Jiang, G. Bin Bian, and Z. Tian, "Removal of artifacts from EEG signals: A review," Sensors, vol. 19, no. 5, 2019. doi: 10.3390/s19050987.
- [12] M. Demuru, S. M. La Cava, S. M. Pani, and M. Fraschini, "A comparison between power spectral density and network metrics: An EEG study," *Biomedical Signal Processing and Control*, vol. 57, 2020. doi: 10.1016/j.bspc.2019.101760.
- [13] R. Wang, J. Wang, H. Yu, X. Wei, C. Yang, and B. Deng, "Power spectral density and coherence analysis of Alzheimer's EEG," *Cognitive neurodynamics*, vol. 9, no. 3, pp. 291–304, 2015. doi: 10.1007/s11571-014-9325-x.
- [14] M. Fathi, Y. Zulkifli, and N. M. Nasir, "Classification of Electromyography Signal of Diabetes using Artificial Neural Networks," *International Journal of Advanced Computer Science and Applications*, vol. 13, no. 11, 2022.
- [15] K. Sivasankari, K. Thanushkodi, and K. Kalaivanan, "Automated Seizure Detection Using Multilayer Feed Forward Network Trained Using Scaled Conjugate Gradient Method," *Physica B: Condensed Matter*, vol. 329, pp. 1554-1555, 2013. doi: 10.1016/S0921.
- [16] M. Fodslette Meiller, "A Scaled Conjugate Gradient Algorithm for Fast Supervised Learning," *Neural networks*, vol.6, no.4, pp. 525-533, 1993.
- [17] N. Konnova, B. Mikhail, and K. Vera, "Application of machine learning algorithms for SCG signal classification," *International Conference on Image, Video Processing and Artificial Intelligence*, SPIE, vol. 11584, pp. 374-379, 2020.
- [17] S. Ahdy, T. Hassan, B. Rahman, R. Sandler and H. Mansy, "Effect of the Initial Condition on SCG Clustering using Unsupervised Machine Learning" *IEEE Signal Processing in Medicine and Biology Symposium* (SPMB, IEEE, pp. 1-5, 2024.
- [18] S. H. Haji, and A. M. Abdulazeez, "Comparison of optimization techniques based on gradient descent algorithm: A review." *PalArch's*

- Journal of Archaeology of Egypt/Egyptology 18, no. 4, pp. 2715-2743.
- [19] A. A. Ariana, I. A. Wisky, N. L. W. S. R. Ginantra, M. R. Firmansyah, and G. S. Daengs, "Performance analysis of scaled conjugate gradient (SCG) algorithm on computing problems," *INTERNATIONAL CONFERENCE OF SNIKOM 2021*, vol. 2798, no. 1, pp. 020060. AIP Publishing LLC, 2023.
- [20] S. Sathyanarayanan and B. R. Tantri, "Confusion matrix-based performance evaluation metrics," *African Journal of Biomedical Research*, 27(4S), pp.4023-4031, 2024.
- [21] E. Manai, M. Mejri, and J. Fattahi, "Confusion Matrix Explainability to Improve Model Performance: Application to Network Intrusion Detection," 10th International Conference on Control, Decision and Information Technologies (CoDIT), pp. 1-5, 2024.